ACS OMEGA

http://pubs.acs.org/journal/acsodf

Article

Improving the Durability and Performance of Sulfonated Poly(arylene ether)s by Introducing 9,10-Dihydro-9-oxa-10-phosphaphenanthrene 10-oxide Structure for Fuel Cell Application

Hyeon-Ho Kang and Dong-Hoon Lee*

Cite This: *ACS Omega* 2021, 6, 35315−35324

Read Online

ACCESS | Metrics & More | Article Recommendations | Supporting Information

ABSTRACT: Polymer electrolyte membranes in which the hydrophilic and hydrophobic domains phase separate exhibit improved properties and stability. Such a phase separation of hydrophilic and hydrophobic domains can be achieved by polymerizing a 9,10-dihydro-9-oxa-10-phosphaphenanthrene 10-oxide-bisphenol A (DOPO-BPA) and 1,4-bis(4-fluorobenzoyl)-benzene (1,4-FBB) monomer. In this work, sulfonated polymer membranes with various degrees of sulfonation (DS) were prepared and their physicochemical and electrochemical properties were studied. In addition, the effect of molecular structure on the durability of the copolymers was investigated. The sulfonated copolymers were characterized by Fourier-transform infrared spectroscopy and proton nuclear magnetic resonance spectroscopy. Then, sulfonated membranes were prepared using these copolymers by the solvent casting method, and their morphologies were investigated by atomic force microscopy. The effect of DS on the thermal, mechanical, and oxidative stabilities, water uptake behavior, and ion-exchange capacity of the membranes was determined. The results showed that compared with the commercially available Nafion 212 polymer electrolyte membrane, the electrolyte membrane based on DOPO-BPA and 1,4-FBB exhibited a lower water uptake and excellent dimensional stability despite having a relatively high ion-exchange capacity. The low water uptake is an important characteristic that ensures the stability of the polymer electrolyte membrane in fuel cell applications.

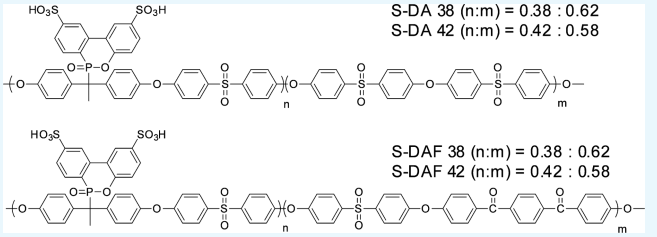

1. INTRODUCTION

Recently, fuel cells have received significant attention worldwide owing to the growing demand for hydrogen fuel as a clean alternative to fossil fuels. Fuel cells can be classified into different types depending on the type of electrolyte used. Among them, polymer electrolyte membrane fuel cells (PEMFCs) are a type of renewable power generation device that generates electricity directly from the chemical energy of fuels via an electrocatalytic reaction.[1−4] A distinguishing feature of PEMFCs that determines their electrochemical performance is the polymer electrolyte membrane (PEM). For efficient functioning, PEMs must have high thermal and mechanical stability, excellent processability, and good water retention ability in low-relative humidity conditions.[5−8] In addition, PEMs must be selectively permeable to small molecules such as ionic species, which exhibit a complex transport behavior, and be particularly conducive to the fast transport of protons; however, they should be impermeable to gases since permeated gases can cause thermal decomposition of the cathode catalyst, thereby deteriorating the fuel cell performance.[9−11]

One of the representative PEMs used in PEMFCs is the aromatic ionomer, perfluorinated sulfonic acid (PFSA).[12−16] PFSA has a C−F backbone, which provides excellent chemical resistance; however, PFSA is difficult to synthesize and expensive.[12,17−19] Other aromatic ionomers have also been used to prepare high-performance materials with good thermodynamic and mechanical properties that are inexpensive and easily synthesizable, modifiable, and processable.[13,20−22] However, most aromatic ionomers have a low conductivity despite having a high ion-exchange capacity (IEC) due to excessive moisture expansion. Additionally, the water swelling of the membrane induces an interfacial resistance due to delamination between the membrane and the electrode, which degrades the cell performance.[23,24]

9,10-Dihydro-9-oxa-10-phosphaphenanthrene 10-oxide-bisphenol A (DOPO-BPA) is an aromatic ionomer with excellent modifiability and processability. It is a cardo polymer, which is a subgroup of polymers that contain carbons arranged in a ring structure in the polymer backbone. These structures are the development of ionic cluster sulfonated polymers to enhance the hydrophilic domain, and exhibit good dimensional stability and high thermal stability.[25−27]

Received: August 5, 2021
Accepted: November 29, 2021
Published: December 14, 2021

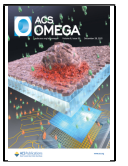

ACS Publications

© 2021 The Authors. Published by American Chemical Society

To improve the properties and stability of the hydrated membranes, proper phase separation of the hydrophilic and hydrophobic domains must be induced.[28−33] Therefore, it is necessary to design a polymer in which the hydrophilic and hydrophobic domains are distinctly separate. This can be accomplished by polymerizing FBB and DOPO structure, which yields a polymer with improved thermal and mechanical properties.[34,35] These membranes exhibit sufficiently high stability at a high IEC.[35−38] 1,4-Bis(4-fluorobenzoyl)benzene (1,4-FBB) and DOPO-BPA were used to induce hydrophilic−hydrophobic phase separation to improve the dimensional stability of the membrane and cell performance.[35]

In this study, sulfonated DOPO-BPA (S-DA) and DOPO-BPA-1,4-FBB (S-DAF) copolymers with different degrees of sulfonation were used to prepare PEM materials for PEMFCs. By synthesizing random copolymers with different numbers of DOPO-BPA groups and controlling the degree of sulfonation, membranes with good dimensional stability and high thermal stability could be obtained owing to the good thermal properties of the DOPO-BPA groups along the copolymer main chain and the sulfonated pendent as well as the aromatic structure. The effect of DOPO and FBB structure on the properties of the copolymer membranes was systematically investigated, and the performance of the PEM was evaluated by applying them to PEMFCs.

2. RESULTS AND DISCUSSION

2.1. Synthesis and Properties of the Monomers and Polymers. 1,4-FBB and DOPO-BPA monomers were successfully synthesized according to the procedures reported in the literature with a modified recrystallization process (see the Experimental Section). The chemical structures of 1,4-FBB and DOPO-BPA were analyzed by proton nuclear magnetic resonance (^{1}H NMR) spectroscopy. In the ^{1}H NMR spectrum of 1,4-FBB, the proton peaks of the aromatic rings appear at 7.89−7.93 ppm, while the four proton peaks of the main aromatic ring appear at 7.18−7.28 ppm (Figure 1). In the ^{1}H-NMR spectrum of DOPO-BPA (Figure 2), the proton peak for the −OH group of DOPO-BPA appears at 9.22 ppm. The signals of the methyl group are split into two peaks with a coupling constant of 17.4 Hz due to J_{P-H} coupling.[42,45]

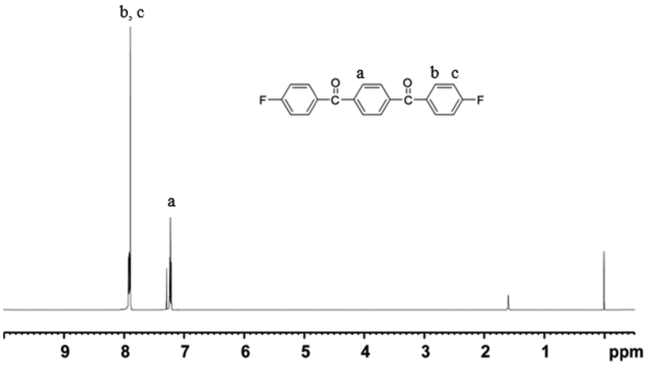

Figure 1. ^{1}H NMR spectrum of the 1,4-FBB monomer.

Figures 3 and 4 show the ^{1}H-NMR spectra of the DOPO-BPA (S-DA 38 and S-DA 42) and DOPO-BPA-1,4-FBB (S-DAF 38 and S-DAF 42) copolymers. The values 38 and 42 in the sample designations denote the degree of sulfonation of the DOPO-BPA monomer. Different S-DA and S-DAF copolymers were prepared by the polycondensation of DOPO-BPA, bis(4-fluorophenyl)sulfone (DFDPS), bis(4-hydroxyphenyl)-sulfone (BHPS), and 1,4-FBB, as shown in Figure 12. The copolymers have a high molecular weight (M_w) ranging from 142,000 to 204,000. The viscosity of S-DA 38 and S-DA 42

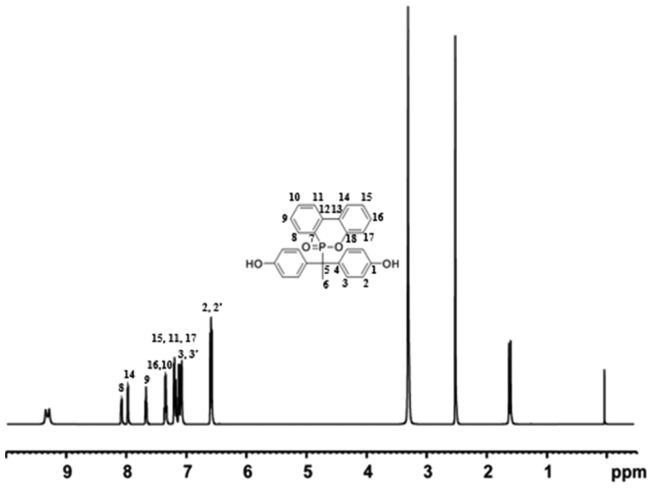

Figure 2. ^{1}H NMR spectrum of the DOPO monomer.

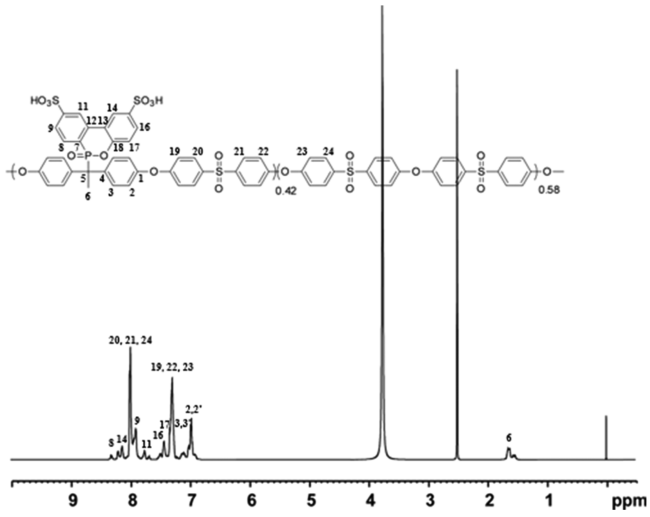

Figure 3. ^{1}H NMR spectrum of the S-DA 42 copolymer.

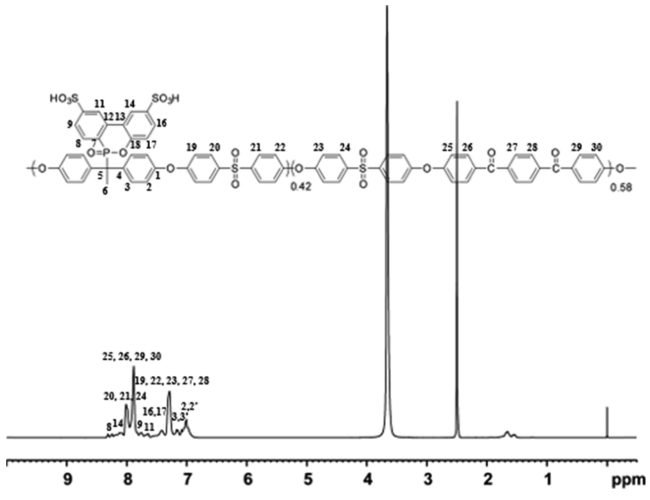

Figure 4. ^{1}H NMR spectrum of the S-DAF 42 copolymer.

https://doi.org/10.1021/acsomega.1c04205
ACS Omega 2021, 6, 35315−35324

varied from 1.52 to 1.59 dL·g^{-1}, while that of S-DAF 38 and S-DAF 42 varied from 0.82 to 1.02 dL·g^{-1}. The chemical structures of the S-DA and S-DAF copolymers were analyzed by FTIR and ^{1}H NMR spectroscopies. Figure 5 shows the

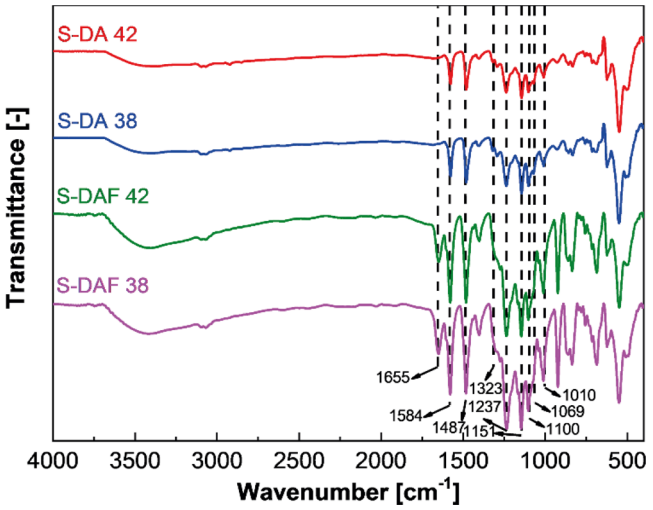

Figure 5. FTIR spectra of S-DA 42, S-DA 38, S-DAF 42, and S-DAF 38 copolymer membranes.

FTIR spectra of the copolymers. In the FTIR spectra of S-DAF 38 and S-DAF 42, the peak at 1655 cm^{-1} corresponds to the carbonyl group (C═O) of 1,4-FBB [33]. In the FTIR spectra of the S-DA and S-DAF copolymers, the peaks at 1584 and 1487 cm^{-1} are assigned to the aromatic ring (C═C) of the DOPO structure,[42,46] while the bands at 1323 and 1151 cm^{-1} arise from P═O and P−O−Ar, respectively.[47,48] The peaks corresponding to P═O stretching vibration overlap with those of C−O−C appearing at 1237 and 1010 cm^{-1}. The peak near 1069 cm^{-1} is attributed to the sulfonic acid groups, while the peak at 1100 cm^{-1} arises from the symmetric sulfur dioxide (O═S═O). In addition, the sulfonated polymers exhibit a wide band from 3200 to 3600 cm^{-1} due to the presence of water and the hydroxyl groups (-OH) of the sulfonic acid moieties. Figures 3 and 4 show the ^{1}H NMR spectra of S-DA and S-DAF with the assignments of all the protons. Owing to the presence of many aromatic protons, the region between 6.5 and 8.5 ppm was assessed, and the signal at 1.62 ppm is attributed to the protons of the methyl group on the aromatic rings. Especially, compared with S-DA42 and S-DAF, the highest chemical shifts at 7.3 and 7.9 ppm are assigned to the proton of C−H in the 1,4-FBB aromatic rings. Thus, ^{1}H NMR and FTIR spectroscopic analyses confirm the site specificity and degree of sulfonation of the well-defined S-DA and S-DAF copolymers.

2.2. Thermal and Mechanical Properties. The thermal stability of S-DA and S-DAF for application as a PEM was investigated by thermogravimetric analysis (TGA) and differential scanning calorimetry (DSC). As shown in Figure 6, all the polymer membranes exhibited typical two-step thermal degradation curves. The initial weight loss step appeared at ∼250 °C, while the second weight loss step, which is related to the thermal degradation of the backbone and sulfonic acid groups,[49−51] appeared at ∼450 °C. DSC data show the typical thermal property of copolymers in Figure S1.

The thermal and mechanical properties of the S-DA and S-DAF membranes are summarized in Table 1. The S-DA and S-

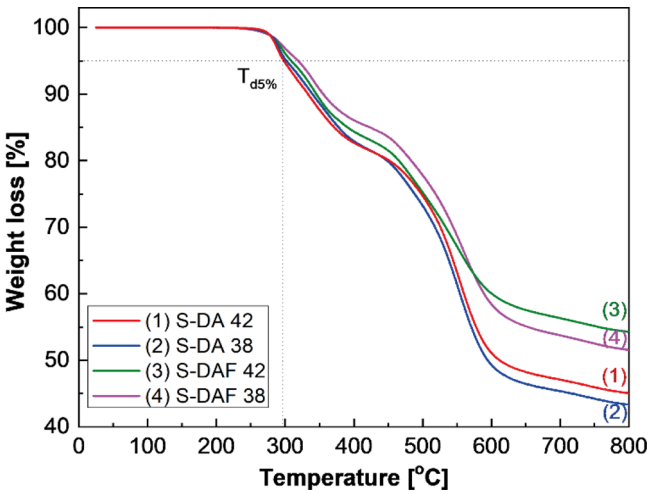

Figure 6. TGA curves of S-DA 42, S-DA 38, S-DAF 42, and S-DAF 38 copolymer membranes.

DAF copolymers displayed excellent thermal stability, as determined from the 5% weight loss temperature ($T_{d5\%}$; Figure 6 and Table 1). $T_{d5\%}$ of the S-DA copolymers was ≥297 °C, while that of the S-DAF copolymers was ≥308 °C. S-DA and S-DAF demonstrated two-step weight loss above 297 and 460 °C, which was attributed to the degradation of the −SO_3H group and the polymer backbone, respectively. Interestingly, the S-DAF copolymers were more thermally stable than the S-DA copolymers; this suggests that the DOPO structure imparts a higher thermal resistance.

The mechanical properties of the S-DA and S-DAF membranes were determined at room temperature under dry conditions. The results are listed in Table 1. As shown in Table 1, the tensile strengths (38.21−44.10 MPa) and Young's moduli (789.3−1116.3 MPa) of the S-DA and S-DAF membranes are much higher than those of the Nafion membranes. Furthermore, the elongations at break of the S-DA and S-DAF membranes (9.90−19.83%) are much lower. This is attributed to the presence of rigid backbone structures in the copolymers, similar to that of other aromatic hydrocarbon polymers reported in the literature. The results indicate that the S-DA and S-DAF membranes are strong and tough enough to be used as PEM materials in PEMFCs.

2.3. Fundamental Characteristics of S-DA and S-DAF Membranes. Water uptake and dimensional stability are closely related to the IEC. In the case of S-DA and S-DAF, the IEC and, hence, the water uptake and dimensional stability depend on the amount of hydrophilic sulfonic acid groups present in the copolymers.[52,53] Membrane water uptake and dimensional swelling are caused by water present in the membrane electrode assembly, which leads to delamination of the membrane electrode and thus reduction in cell durability.[54,55] In this study, the IEC values of S-DA and S-DAF, determined by acid−base titration, are close to the theoretical IEC values (Table 2). As shown in Figure 7, the IEC of S-DAF is lower than that of S-DA although they have the same degree of sulfonation. This is because of the enhanced stability of the hydrophobic segments due to the presence of FBB domains in S-DAF, which render the copolymer membrane more resistant to water absorption.

The water uptake and dimensional swelling were measured in deionized (DI) water. At room temperature, the water uptake of the S-DA 38 and S-DA 42 membranes was 22.14 and

https://doi.org/10.1021/acsomega.1c04205
ACS Omega 2021, 6, 35315−35324

Table 1. Thermal and Mechanical Properties of S-DA and S-DAF Membranes

polymer	T_g	$T_{d5\%}$[a]	tensile strength at break[b] (MPa)	Young's modulus[b] (MPa)	elongation at break[b] (%)	oxidative stability[c] (%)	proton conductivity (S cm^{-1}) 30 °C	proton conductivity (S cm^{-1}) 80 °C
S-DA 42	207	297	42.32	842	9.90	76	0.07	0.18
S-DA 38	192	301	44.10	861	9.95	84	0.05	0.17
S-DAF 42	213	308	38.21	789.3	18.86	>99	0.055	0.139
S-DAF 38	198	318	38.69	1116.3	19.83	>99	0.039	0.099
Nafion 212						100	0.09	0.18

[a]The temperature at which 5% weight loss of the membrane occurs, as measured by TGA (acid form). [b]Samples were dried at 120 °C, and measurement was carried out at a crosshead speed of 2 mm·min^{-1} at room temperature (25 °C). [c]The weight of the membrane soaked in Fenton's reagent (3 wt % H_2O_2 and 2 ppm $FeSO_4$) at 80 °C for 2 h was measured.

Table 2. Fundamental Properties of S-DA and S-DAF Membranes

polymer	$[\eta]$[a] (dL g^{-1})	M_w (×10^4 g mol^{-1})	theoretical IEC (meq g^{-1})	titrated IEC (meq g^{-1})	water uptake (%) 25 °C	water uptake (%) 80 °C[b]	dimensional swelling (%) Δt 25 °C	dimensional swelling (%) Δt 80 °C	dimensional swelling (%) Δl 25 °C	dimensional swelling (%) Δl 80 °C
S-DA 42	1.59	12.1	1.38	1.37	31.03	94.12	29.61	40.84	21.74	31.64
S-DA 38	1.52	20.4	1.21	1.21	22.14	63.19	17.93	25.27	11.52	17.36
S-DAF 42	1.02	14.6	1.26	1.29	8.70	30.43	3.31	10.05	2.44	11.48
S-DAF 38	0.82	14.2	1.19	1.18	7.14	20.00	2.75	8.88	2.06	6.12
Nafion 212			0.96	0.96	30.60	50.00[c]	17.70		25.3	

[a]Intrinsic viscosity in DMSO (0.5 g·dL^{-1}) at 30 °C. [b]The dry membrane was soaked in water at 80 °C for 24 h, and then, its weight was measured. [c]The dry membrane was soaked in water at 100 °C for 1 h, and then, its weight was measured

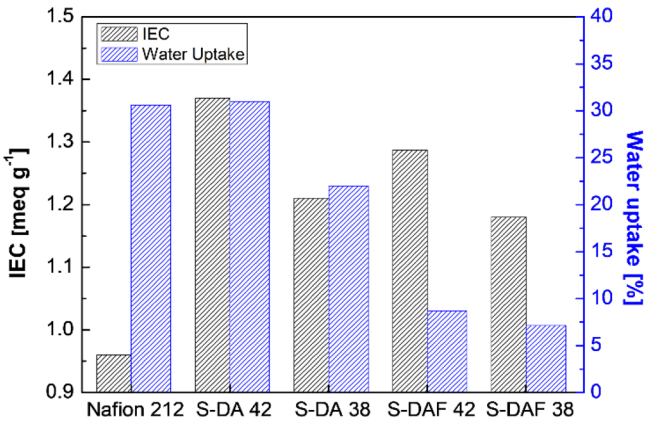

Figure 7. IEC and water uptake of S-DA 42, S-DA 38, S-DAF 42, and S-DAF 38 copolymer membranes and Nafion 212.

31.03%, respectively, while that of the S-DAF 38 and S-DAF 42 membranes was 7.14 and 8.70%, respectively. As shown in Table 2, the trend of water uptake measured at 80 °C is consistent with the trend of water uptake at 25 °C. Although the S-DA and S-DAF copolymers have the same degree of sulfonation, the water uptake of the S-DAF membranes was significantly lower than that of the S-DA membranes. This phenomenon also may be profit from the promoted phase separation morphology attributed to the hydrophobicity of the FBB structure isolated from the main structure.

The dimensional change of the membranes due to water uptake was also measured in DI water. The dimensional changes and test conditions are presented in Table 2. Regardless of the polymer type, the dimensional swelling and water uptake increased with an increase in the degree of sulfonation. This is proportional to the IEC, which indicates an absolute increase in the amount of hydrophilic sulfonic acid groups. In addition, the dimensional swelling in the through-plane (Δt) direction is larger than the dimensional swelling in the in-plane (Δl) direction. The S-DAF membranes exhibited excellent dimensional stability even though their degree of sulfonation is the same as that of the S-DA membranes. The result suggests that the FBB structure present in the S-DAF copolymer improved the dimensional stability of the membranes.

As shown in Table 1, the oxidative stabilities of the S-DA, S-DAF, and Nafion 212 membranes were measured by Fenton's test, which mimics the harsh conditions of fuel cell operation that leads to accelerated degradation. In Fenton's test, the samples were immersed in Fenton's reagent at 80 °C for 2 h. The S-DA membranes exhibited a low oxidative stability of 76 and 84%, while the S-DAF membranes exhibited excellent stability of >99%. The result shows that the oxidative stability decreased with an increase in the number of hydrophilic segments in the copolymer. Hence, the S-DAF membranes exhibited excellent oxidative stability.[56−58]

2.4. Proton Conductivity and Morphology. The proton conductivity of membranes is closely related to their water sorption property. The absorption of a certain amount of water is beneficial to the formation of hydrophilic domains inside the membrane. However, excessive swelling can dilute the concentration of ion-conducting groups, thereby disrupting the channel of hydrophobic domains, which results in poor membrane durability. The effect of relative temperature on the proton conductivity of the membranes with different degrees of sulfonation was investigated, and the results are shown in Figure 8. The proton conductivity of the membranes was measured using a four-probe electrode AC impedance spectroscope. Figure 8 shows the proton conductivities of the membranes measured in DI water in the temperature range

https://doi.org/10.1021/acsomega.1c04205
ACS Omega 2021, 6, 35315−35324

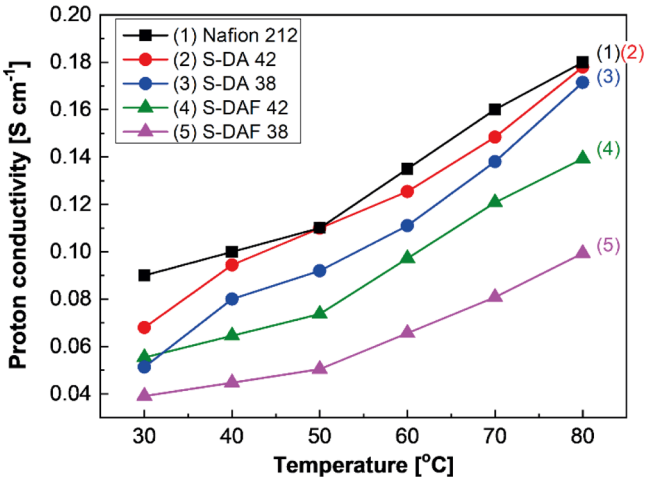

Figure 8. Proton conductivity of S-DA 42, S-DA 38, S-DAF 42, and S-DAF 38 copolymer membranes and Nafion 212.

of 30−80 °C at 10 °C intervals. At 80 °C, the proton conductivities of S-DA 38 (0.17 S·cm^{-1}) and S-DA 42 (0.18 S·cm^{-1}) were slightly lower than those of the Nafion 212 membrane. With an increase in temperature from 30 to 80 °C, the proton conductivity of the membranes increased by >50%, which is attributed to membrane hydration and water diffusion facilitated by the high temperature. At 80 °C, the proton conductivities of S-DAF 38 (0.099 S·cm^{-1}) and S-DAF 42 (0.139 S·cm^{-1}) with FBB structures were significantly lower than those of the S-DA membranes. The low proton conductivity of the membranes is attributed to their relatively low hydration level and reduced water swelling, as discussed above.

Furthermore, the morphology of the membranes was analyzed by atomic force microscopy (AFM) and transmission electron microscopy (TEM). As shown in the AFM images in Figure 9, the hydrophilic−hydrophobic domains on the surface of the S-DA and S-DAF membranes can be identified as brightly marked hydrophilic domains located between the hydrophobic domains. Compared with the S-DA membranes, the S-DAF membranes exhibit higher connectivity between the hydrophilic domains. The TEM image also shows a similar morphology to the AFM image in Figure S2. The proton conductivity of the S-DAF membranes is lower than that of the S-DA membranes even though the hydrophilic domains are well connected in the former. This is attributed to the lower number of sulfonic acid groups per unit mass of the S-DAF membranes due to their low IEC at the same degree of sulfonation as that of the S-DA membranes (Table 2), which decreases the proton conductivity.

2.5. PEMFC Performance. To evaluate the applicability of the copolymer membranes as PEMs in PEMFCs, membrane electrode assemblies (MEAs) were fabricated using the copolymer membranes by the hot-pressing technique and assembled into a single cell. The performance of the PEMFCs employing the S-DA and S-DAF membranes is shown in Figure 10. All the membrane samples exhibit similar polarization behaviors. The intrinsic ohmic resistance affects activation and leads to a low output upon application of a load to a system. At a current density of 600 mA·cm^{-2}, the power density of S-DAF 42 was higher than that of the Nafion 212 membrane. The maximum power densities of the S-DA 38, S-DA 42, S-DAF 38, S-DAF 42, and Nafion 212 membranes were approximately 460, 490, 460, 480, and 430 mW·cm^{-2}, respectively. Furthermore, at high current densities of over 800 mA·cm^{-2}, the current−voltage curves of the membranes were more stable than those of the Nafion 212 membrane. This is due to the FBB structure of the S-DAF membranes that imparts excellent dimensional stability and reduces water uptake.[59] Consequently, the PEMFC performance of the S-DAF membranes was better than that of the S-DA membranes. This suggests that membrane FBB structures have improved cell performance and long-term stability. The result indicates that our copolymer membranes have significant application potential as PEMs in PEMFCs.

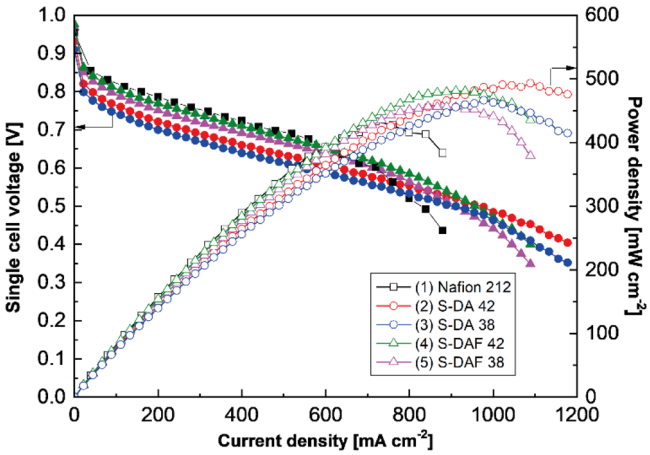

Figure 10. H_2/Air PEMFC performance of S-DA 42, S-DA 38, S-DAF 42, and S-DAF 38 copolymer membranes and Nafion 212.

3. CONCLUSIONS

In this study, S-DA and S-DAF copolymer membranes were designed, successfully synthesized, and used as PEMs in PEMFCs. NMR and FTIR spectroscopic analyses confirmed

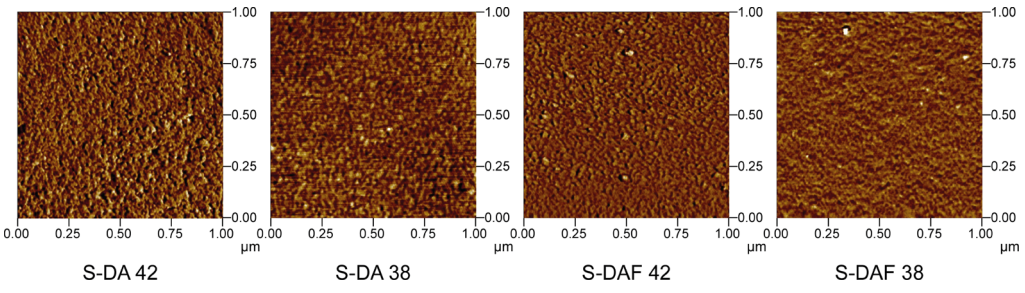

Figure 9. AFM images of S-DA 42, S-DA 38, S-DAF 42, and S-DAF 38 copolymer membranes.

https://doi.org/10.1021/acsomega.1c04205
ACS Omega 2021, 6, 35315−35324

the successful synthesis of the S-DA and S-DAF copolymers. Because of the FBB structure, the S-DAF membranes were more thermally stable than the S-DA membranes. Compared with the Nafion 212 membrane, the S-DA and S-DAF membranes exhibited a lower water uptake and excellent dimensional stability despite having a higher IEC. Thus, the performance of the S-DA and S-DAF membranes as PEMs in PEMFCs was better and more stable than that of the Nafion 212 membrane at high current densities. This study demonstrates that PEM materials bearing DOPO and FBB structure impart long-term operational stability to fuel cells.

4. EXPERIMENTAL SECTION

4.1. Materials. 9,10-Dihydro-9-oxa-10-phosphaphenanthrene 10-oxide (DOPO, 97%), *p*-toluene sulfonic acid monohydrate, and phenol were purchased from TCI Chemicals (Japan). 4'-Hydroxyacetophenone (98%) was purchased from Acros Organics (USA). Fluorobenzene (99%), terephthaloyl chloride (>99%), calcium hydride (95%), potassium carbonate (99%), and sulfonic acid (95%) were purchased from Merck Co. (USA). Dimethylacetamide (DMAc) and toluene were purified by drying over calcium hydride under continuous stirring for 1 day and were distilled before use. The other solvents, i.e., methanol, acetone, and DI water, were used as received.

4.2. Synthesis of the 1,4-FBB Monomer. The 1,4-FBB monomer was synthesized following the procedures reported in the literature with slight modification (Figure 1).[39−41] Terephthaloyl chloride (18.3 g, 0.09 mol) and fluorobenzene (33.9 mL, 0.36 mol) were mixed, and $AlCl_3$ (13.3 g, 0.1 mol) was slowly added to the mixture at 25 °C. Since the reaction is exothermic, the temperature was slowly increased to 60 °C after sufficient stabilization. The reaction was allowed to proceed for 4 h at 80 °C. The mixture was then cooled to 25 °C and poured into an aqueous hydrochloric acid solution (3 vol %). The resulting suspension was stirred for at least 12 h and distilled to eliminate excess fluorobenzene, and the remaining solids were collected by filtration. The collected residue was then rinsed several times with methanol and aqueous hydrochloric acid solution (3 vol %). The product was recrystallized from DMAc, and the obtained pastel green powder was dried in a vacuum oven at 150 °C. Yield: 34 g (65%); melting point 221−222 °C. ^{1}H NMR (600 MHz, $CDCl_3$) δ (ppm): 7.18−7.28 (m, 4H), 7.86−7.93 (m, 6H).

4.3. Synthesis of the DOPO-BPA Monomer. The DOPO-BPA monomer was synthesized according to reported procedures (Figure 11).[42,43] Briefly, DOPO (10.81 g, 0.05 mol), 4-hydroxyacetophenone (6.81 g, 0.05 mol), p-TSA (0.432 g, 0.0025 mol), and phenol (14.11 g, 0.15 mol) were added to a three-neck round-bottom flask and stirred for 10 h at 60 °C. The obtained DOPO-BPA was filtered with methanol and dried in an oven at 100 °C. The product was then recrystallized from methanol and dried in a vacuum oven at 120 °C. Yield: 21 g (68%); melting point 359−360 °C. ^{1}H NMR (600 MHz, $CDCl_3$) δ (ppm): 1.51−1.65 (m, 3H), 6.51−6.61 (m, 2H), 7.05−7.21 (m, 7H), 7.34−7.39 (m, 2H), 7.70−7.78 (m, 1H), 8.01−8.08 (m, 1H), 8.12−8.19 (m, 1H), 9.36−9.47 (d, 2H).

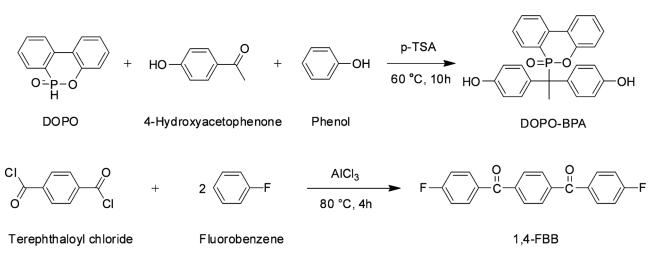

Figure 11. Synthesis of 1,4-FBB and DOPO-BPA monomers.

4.4. Synthesis and Sulfonation of Polymers. *4.4.1. Synthesis of the DOPO-BPA Copolymer (DA Copolymer).* The DA copolymer was synthesized by a typical polycondensation process (Figure 12). DOPO-BPA (1.798 g, 4.2 mmol), DFDPS (2.543 g, 10 mmol), BHPS (1.452 g, 5.8 mmol), K_2CO_3 (1.294 g, 9.63 mmol), DMAc (18 mL), and toluene (9 mL) were added to a three-neck round-bottom flask equipped with a Dean−Stark trap, N_2 inlet/outlet, and condenser. The mixture was heated to 150 °C for 4 h to remove water. The temperature was then raised to 180 °C for an additional 8 h to distill off toluene and remove remaining water. The resulting mixture was then poured into a methanol (400 mL)/water (600 mL) solution and filtered. Finally, the product was rinsed with water and dried in a vacuum oven at 100 °C for 24 h.

4.4.2. Synthesis of the DOPO-BPA Copolymer (DAF Copolymer). The DAF copolymer was synthesized by a typical polycondensation process (Figure 12). DOPO-BPA (1.798 g, 4.2 mmol), DFDPS (1.068 g, 4.2 mmol), BHPS (1.452 g, 5.8 mmol), 1,4-FBB (1.869 g, 5.8 mmol), K_2CO_3 (1.382 g, 1.00 mmol), DMAc (18 mL), and toluene (9 mL) were added to a three-neck round-bottom flask equipped with a Dean−Stark trap, N_2 inlet/outlet, and condenser. The mixture was refluxed at 150 °C for 4 h to remove water and then heated to 180 °C for 8 h to distill off toluene and water. The resulting mixture was then poured into a methanol (400 mL)/water (600 mL) solution and filtered. Finally, the product was rinsed with water and dried in a vacuum oven at 100 °C for 24 h.

4.4.3. Sulfonation of the Copolymer. The dried polymer (1.00 g) was added to a three-neck round-bottom flask, completely dissolved in concentrated H_2SO_4 (15 mL) under a nitrogen atmosphere, and then kept at 30 °C for 6 h. The solution was then slowly poured into ice water, and the resulting precipitate was repeatedly rinsed with water to eliminate any acid residue.

4.5. Preparation of Membranes by Solvent Casting. To prepare thin membrane films, the polymers were dissolved in DMSO (10% w/v) and filtered through a PTFE syringe filter. The filtrates were evenly poured into hydrophilic glass plates and cast using a doctor blade. The films were first dried at 60 °C for 12 h and then dried in a vacuum oven at 120 °C for 24 h.

4.6. Characterization of Polymer Membranes. The polymers dissolved in $CDCl_3$-d_1 and DMSO-d_6 were analyzed by ^{1}H NMR spectroscopy (Bruker Avance, 600 MHz) using tetramethylsilane as the internal standard. FTIR spectroscopy (Perkin Elmer, Frontier) was performed in the wavenumber range of 4000−400 cm^{-1} in the ATR mode at a resolution of 4 cm^{-1}. Gel permeation chromatography (GPC; Waters, Alliance e2695) was performed in DMSO with a flow rate of 1.0 mL·min^{-1}. The average molecular weights were calibrated with polystyrene standards. The prepared membranes were dissolved in DMSO at a concentration of 0.5 g·dL^{-1}, and the intrinsic viscosity was measured at 30 °C using an Ubbelohde viscometer. DSC (Mettler Toledo, DSC A851e) was performed at a heating rate of 10 °C·min^{-1} in the temperature range of 50−300 °C under an N_2 atmosphere. TGA (Mettler

https://doi.org/10.1021/acsomega.1c04205
ACS Omega 2021, 6, 35315−35324

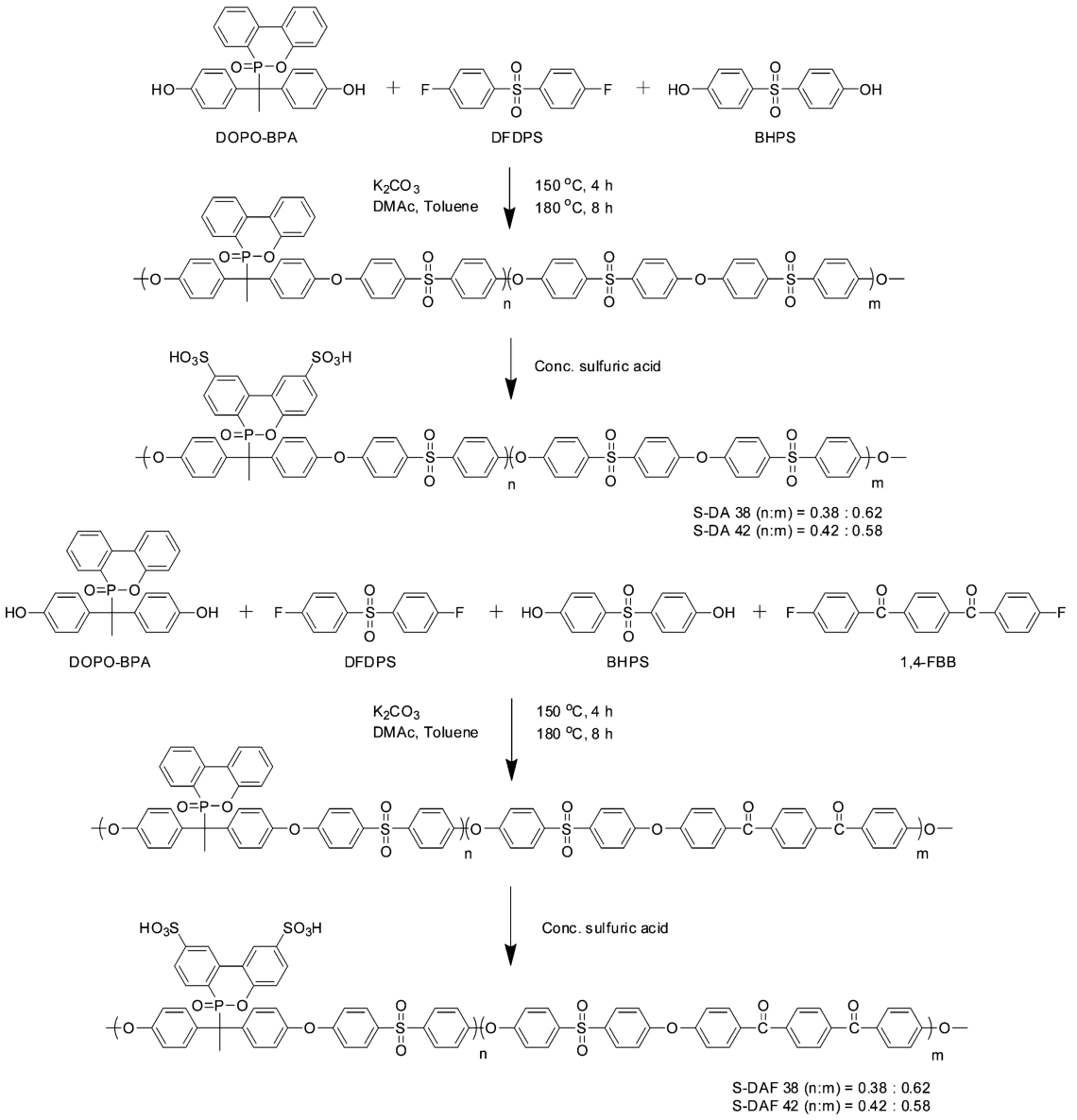

Figure 12. Synthesis of S-DA 38, S-DA 42, S-DAF 38, and S-DAF 42 copolymer membranes with different degrees of sulfonation.

Toledo, TGA A851e) was performed to evaluate the thermal stability of the membranes. First, the dried membranes were loaded into a TGA instrument and held at 160 °C for 15 min. After cooling the membranes under an N_2 atmosphere, the membranes were heated to 800 °C at a rate of 10 °C·min^{-1}, and the temperature at which 5% weight loss occurred for each membrane was recorded. The surface morphology of the prepared membranes was analyzed by AFM (PSIA XE100) performed in the noncontact mode using P/N 910 M-NCHR tips. Tapping-mode AFM was conducted using a Digital Instrument (SII-NT SPA400) with microfabricated cantilevers and a force constant of ∼20 N·m^{-1}.

4.7. Weight-Based Ion-Exchange Capacity (IEC_w). The weight-based ion-exchange capacity (IEC_w) was determined by the acid−base titration of the sulfonated polymers. First, the weight of the dry membranes in their acid form was measured. Then, the samples were immersed in a 2.0 mol·L^{-1} NaCl solution for 24 h. The NaCl solution was then replaced with a HCl solution, and acid−base titration was carried out using 0.05 mol·L^{-1} NaOH solution. The IEC_w was calculated as follows:

$$IEC_w = \frac{V_{NaOH} \times C_{NaOH}}{W_{dry}}$$

where V_{NaOH} is the volume of the NaOH solution, C_{NaOH} is the concentration of the NaOH solution, and W_{dry} is the weight of the dried membrane.

4.8. Dimensional Change and Water Uptake. To determine the change in the length and thickness of the membrane samples, the membranes were first soaked in DI water at a constant temperature for 24 h and their length and thickness were measured. The membrane samples were then dried in a vacuum oven at 100 °C for 24 h, and the length and thickness of the dried membranes were measured. Dimensional changes were calculated as follows:

$$\Delta l\ (\%) = \frac{L_{wet} - L_{dry}}{L_{dry}} \times 100$$

https://doi.org/10.1021/acsomega.1c04205
ACS Omega 2021, 6, 35315−35324

and

$$\Delta t\ (\%) = \frac{T_{wet} - T_{dry}}{T_{dry}} \times 100$$

where T_{wet} and L_{wet} are the thickness and length of the membranes in the wet state, respectively, and T_{dry} and L_{dry} are the thickness and length of the membranes in the dry state, respectively. The change in length (Δl) and change in thickness (Δt) of the membranes are represented as percentages.

The water uptake of the samples was calculated by measuring the dry and wet weights of the samples. The water uptake of the samples was calculated as weight percentage by the following equation:

$$\text{Water uptake}\ (\%) = \frac{W_{wet} - W_{dry}}{W_{dry}} \times 100$$

where W_{wet} and W_{dry} are the weights of the wet and dried samples, respectively.

4.9. Oxidative Stability. The accelerated oxidative stability test is generally performed using Fenton's reagent (3% H_2O_2 containing 2 ppm Fe^{2+}). The membranes were immersed in Fenton's reagent at 80 °C for 2 h, and the weight of the remaining membrane was measured.

4.10. Mechanical Properties. The tensile strength, Young's modulus, and elongation at break were measured using a Universal Testing Machine (UTM; Ametek, Lloyd instruments) at a crosshead speed of 2 mm·min^{-1}. The samples were cut with a membrane thickness of ∼25 μm into 10 mm × 40 mm pieces. Average values were obtained after measuring at least 10 specimens of each membrane sample.

4.11. Proton Conductivity. Electrochemical impedance spectroscopy (EIS) was performed using a potentiostat (Biologic, VMP3). The samples (1 cm × 4 cm) were placed on four platinum electrodes, fixed using a PTFE clamp, and immersed in DI water. The proton conductivity (σ, S·cm^{-1}) was obtained from the following equation:

$$\sigma = \frac{L}{RA}$$

where R is the ohmic resistance, L is the distance between the platinum electrodes, and A is the exposed surface area of the sample.[44]

4.12. Fabrication of MEA and Evaluation of PEMFC Performance. MEAs were fabricated on both sides of the electrodes by the decal transfer method. The catalyst layer of both the electrodes was prepared using 70 wt % Pt/C (Hispec 13100, Johnson Matthey Inc.), with Pt loadings of 0.2 mg·cm^{-2} at the anode and 0.4 mg·cm^{-2} at the cathode. MEAs were prepared by applying a pressure of 10 MPa at 130 °C for 5 min. Wet-proofed Toray carbon sheet (TGPH-060, Toray Inc.) was used for the gas diffusion layer (GDL) at the anode side, whereas Sigracet carbon paper (SGL-25 BC, Sigracet Inc.) was used for the GDL at the cathode side. GDLs were implemented on both sides of the electrodes in the MEAs.

After the MEAs were assembled into a single cell with an active area of 9 cm^2, the MEAs were hydrated by supplying fully humidified N_2 gas into the single cell for 2 h. To evaluate the single cell, H_2 at 1.5 bar was supplied to the anode side and air at 2.0 bar was supplied to the cathode side in the fully humidified N_2 gas. The operation temperature was set at 70 °C. After activating the MEAs, current−voltage curves were measured in the constant current mode starting at the open-circuit voltage using a PEMFC test station (Fuel Cell Test Station, Scitech Korea Inc.) at 70 °C.

■ ASSOCIATED CONTENT

Supporting Information

The Supporting Information is available free of charge at https://pubs.acs.org/doi/10.1021/acsomega.1c04205.

DSC data of DAF 42 and S-DAF 42 copolymers; TEM image of the S-DAF 42 copolymer; EIS analysis of S-DAF 42 and Nafion 212 membranes on MEA (PDF)

■ AUTHOR INFORMATION

Corresponding Author

Dong-Hoon Lee − *Department of Chemical Engineering, Wonkwang University, Iksan, Jeonbuk 54538, Republic of Korea;* orcid.org/0000-0002-1599-5122; Email: merits928@wku.ac.kr

Author

Hyeon-Ho Kang − *Department of Chemical Engineering, Wonkwang University, Iksan, Jeonbuk 54538, Republic of Korea*

Complete contact information is available at: https://pubs.acs.org/10.1021/acsomega.1c04205

Author Contributions

All authors have given approval to the final version of the manuscript.

Notes

The authors declare no competing financial interest.

■ ACKNOWLEDGMENTS

This work was supported by Wonkwang University.

■ ABBREVIATIONS

1,4-FBB, 1,4-bis(4-fluorobenzoyl)benzene; ^{1}H NMR, proton nuclear magnetic resonance; AFM, atomic force microscopy; BHPS, bis(4-hydroxyphenyl)sulfone; DFDPS, bis(4-fluorophenyl)sulfone; DMAc, dimethylacetamide; DOPO-BPA, 9,10-dihydro-9-oxa-10-phosphaphenanthrene 10-oxide-bisphenol A; FTIR, Fourier-transform infrared; IEC, ion-exchange capacity; MEA, membrane electrode assembly; PEMFC, polymer electrolyte membrane fuel cell; PFSA, perfluorinated sulfonic acid; $T_{d5\%}$, 5% weight loss temperature

■ REFERENCES

(1) Staffell, I.; Scamman, D.; Velazquez Abad, A.; Balcombe, P.; Dodds, P. E.; Ekins, P.; Shah, N.; Ward, K. R. The role of hydrogen and fuel cells in the global energy system. *Energy Environ. Sci.* **2019**, *12*, 463−491.

(2) Badwal, S. P. S.; Giddey, S. S.; Munnings, C.; Bhatt, A. I.; Hollenkamp, A. F. Emerging electrochemical energy conversion and storage technologies. *Front. Chem.* **2014**, *2*, 79.

(3) Manthiram, A.; Vadivel Murugan, A.; Sarkar, A.; Muraliganth, T. Nanostructured electrode materials for electrochemical energy storage and conversion. *Energy Environ. Sci.* **2008**, *1*, 621−638.

(4) Zhang, H.; Shen, P. K. Recent development of polymer electrolyte membranes for fuel cells. *Chem. Rev.* **2012**, *112*, 2780−2832.

(5) *Proton Exchange Membrane Fuel Cells: Materials Properties and Performance*, 1st ed.; Wilkinson, D. P.; Zhang, J.; Hui, R.; Fergus, J.; Li, X., Eds.; CRC Press: Boca Raton, 2009, pp. 107−137.

(6) Elabd, Y. A.; Hickner, M. A. Block copolymers for fuel cells. *Macromolecules* **2011**, *44*, 1−11.
(7) Subianto, S.; Pica, M.; Casciola, M.; Cojocaru, P.; Merlo, L.; Hards, G.; Jones, D. J. Physical and chemical modification routes leading to improved mechanical properties of perfluorosulfonic acid membranes for PEM fuel cells. *J. Power Sources* **2013**, *233*, 216−230.
(8) Han, M.; Zhang, G.; Shao, K.; Li, H.; Zhang, Y.; Li, M.; Wang, S.; Na, H. Carboxyl-terminated benzimidazole-assisted cross-linked sulfonated poly(ether ether ketone)s for highly conductive PEM with low water uptake and methanol permeability. *J. Mater. Chem.* **2010**, *20*, 3246−3252.
(9) Le, N. L.; Nunes, S. P. Materials and membrane technologies for water and energy sustainability. *Sustain. Mater. Technol.* **2016**, *7*, 1−28.
(10) Li, Y.; Wang, S.; He, G.; Wu, H.; Pan, F.; Jiang, Z. Facilitated transport of small molecules and ions for energy-efficient membranes. *Chem. Soc. Rev.* **2015**, *44*, 103−118.
(11) Klingele, M.; Breitwieser, M.; Zengerle, R.; Thiele, S. Direct deposition of proton exchange membranes enabling high performance hydrogen fuel cells. *J. Mater. Chem. A* **2015**, *3*, 11239−11245.
(12) Einsla, M. L.; Kim, Y. S.; Hawley, M.; Lee, H.-S.; McGrath, J. E.; Liu, B.; Guiver, M. D.; Pivovar, B. S. Toward improved conductivity of sulfonated aromatic proton exchange membranes at low relative humidity. *Chem. Mater.* **2008**, *20*, 5636−5642.
(13) Pang, J.; Shen, K.; Ren, D.; Feng, S.; Wang, Y.; Jiang, Z. Polymer electrolyte membranes based on poly(arylene ether)s with penta-sulfonated pendent groups. *J. Mater. Chem. A* **2013**, *1*, 1465−1474.
(14) Casciola, M.; Alberti, G.; Sganappa, M.; Narducci, R. On the decay of Nafion proton conductivity at high temperature and relative humidity. *J. Power Sources* **2006**, *162*, 141−145.
(15) Tang, Y.; Zhang, J.; Song, C.; Liu, H.; Zhang, J.; Wang, H.; Mackinnon, S.; Peckham, T.; Li, J.; McDermid, S.; Kozak, P. Temperature dependent performance and in situ AC impedance of high-temperature PEM fuel cells using the Nafion-112 membrane. *J. Electrochem. Soc.* **2006**, *153*, A2036.
(16) Wang, C.-Y. Fundamental models for fuel cell engineering. *Chem. Rev.* **2004**, *104*, 4727−4765.
(17) Peighambardoust, S. J.; Rowshanzamir, S.; Amjadi, M. Review of the proton exchange membranes for fuel cell applications. *Int. J. Hydrogen Energy* **2010**, *35*, 9349−9384.
(18) Kim, S.; Hong, I. Effects of humidity and temperature on a proton exchange membrane fuel cell (PEMFC) stack. *J. Ind. Eng. Chem.* **2008**, *14*, 357−364.
(19) Peckham, T. J.; Holdcroft, S. Structure-morphology-property relationships of non-perfluorinated proton-conducting membranes. *Adv. Mater.* **2010**, *22*, 4667−4690.
(20) Park, C. H.; Lee, C. H.; Guiver, M. D.; Lee, Y. M. Sulfonated hydrocarbon membranes for medium-temperature and low-humidity proton exchange membrane fuel cells (PEMFCs). *Prog. Polym. Sci.* **2011**, *36*, 1443−1498.
(21) Budy, S. M.; Loy, D. A. Highly sulfonated polyelectrolytes through Friedel-Crafts sulfonylation of polyarylenes. *J. Polym. Sci., Part A: Polym. Chem.* **2014**, *52*, 1381−1384.
(22) Danyliv, O.; Gueneau, C.; Iojoiu, C.; Cointeaux, L.; Thiam, A.; Lyonnard, S.; Sanchez, J.-Y. Polyaromatic ionomers with a highly hydrophobic backbone and perfluorosulfonic acids for PEMFC. *Electrochim. Acta* **2016**, *214*, 182−191.
(23) Gross, M.; Maier, G.; Fuller, T.; MacKinnon, S.; Gittleman, C. Design rules for the improvement of the performance of hydrocarbon-based membranes for proton exchange membrane fuel cells (PEMFC). In *Handbook of Fuel Cells*; Wiley, 2010, pp. 1−17.
(24) Rama, P.; Chen, R.; Andrews, J. A review of performance degradation and failure modes for hydrogen-fuelled polymer electrolyte fuel cells. *Proc. Inst. Mech. Eng., Part A* **2008**, *222*, 421−441.
(25) Miyatake, K.; Bae, B.; Watanabe, M. Fluorene-containing cardo polymers as ion conductive membranes for fuel cells. *Polym. Chem.* **2011**, *2*, 1919−1929.
(26) Han, G. L.; Zhang, Q. G.; Liu, Q. L. Separation of methanol/methyl tert-butyl ether using sulfonated polyarylethersulfone with cardo (SPES-C) membranes. *J. Membr. Sci.* **2013**, *430*, 180−187.
(27) Gao, N.; Zhang, F.; Zhang, S.; Liu, J. Novel cardo poly(arylene ether sulfone)s with pendant sulfonated aliphatic side chain for proton exchange membranes. *J. Membr. Sci.* **2011**, *372*, 49−56.
(28) Fujimoto, C. H.; Hickner, M. A.; Cornelius, C. J.; Loy, D. A. Ionomeric poly(phenylene) prepared by Diels-Alder polymerization: Synthesis and physical properties of a novel polyelectrolyte. *Macromolecules* **2005**, *38*, 5010−5016.
(29) Matsumoto, K.; Higashihara, T.; Ueda, M. Locally and densely sulfonated poly(ether sulfone)s as proton exchange membrane. *Macromolecules* **2009**, *42*, 1161−1166.
(30) Matsumura, S.; Hlil, A. R.; Lepiller, C.; Gaudet, J.; Guay, D.; Hay, A. S. Ionomers for proton exchange membrane fuel cells with sulfonic acid groups on the end groups: Novel linear aromatic poly(sulfide-ketone)s. *Macromolecules* **2008**, *41*, 277−280.
(31) Lin, L.; Chen, Z.; Zhang, Z.; Feng, S.; Liu, B.; Zhang, H.; Pang, J.; Jiang, Z. New comb-shaped ionomers based on hydrophobic poly(aryl ether ketone) backbone bearing hydrophilic high concentration sulfonated micro-cluster. *Polymer* **2016**, *96*, 188−197.
(32) Skalski, T. J. G.; Britton, B.; Peckham, T. J.; Holdcroft, S. Structurally-defined, sulfo-phenylated, oligophenylenes and polyphenylenes. *J. Am. Chem. Soc.* **2015**, *137*, 12223−12226.
(33) Feng, S.; Wang, G.; Zhang, H.; Pang, J. Graft octa-sulfonated poly(arylene ether) for high performance proton exchange membrane. *J. Mater. Chem. A* **2015**, *3*, 12698−12708.
(34) Lin, C. H.; Lin, C. H. Synthesis and properties of polyimides derived from 1,4-bis(4-aminophenoxy)-2-(6-oxido-6H-dibenz[c,e][1,2]oxaphosphorin-6-yl) phenylene. *J. Polym. Sci., Part A: Polym. Chem.* **2007**, *45*, 2897−2912.
(35) Jeong, J.-E.; Kim, D.-H.; Lee, D.-H. Preparation and characterization of sulfonated semi-crystalline poly(arylene ether)s containing 1,4-FBB moiety as proton exchange membrane fuel cells. *Int. J. Hydrogen Energy* **2018**, *43*, 23004−23013.
(36) Yang, A. C. C.; Narimani, R.; Zhang, Z.; Frisken, B. J.; Holdcroft, S. Controlling crystallinity in graft ionomers, and its effect on morphology, water sorption, and proton conductivity of graft ionomer membranes. *Chem. Mater.* **2013**, *25*, 1935−1946.
(37) Kim, D.-H.; Park, I. K.; Lee, D.-H. Fluorinated sulfonated poly(arylene ether)s bearing semi-crystalline structures for highly conducting and stable proton exchange membranes. *Int. J. Hydrogen Energy* **2020**, *45*, 23469−23479.
(38) Hamada, T.; Hasegawa, S.; Fukasawa, H.; Sawada, S.; Koshikawa, H.; Miyashita, A.; Maekawa, Y. Poly(ether ether ketone) (PEEK)-based graft-type polymer electrolyte membranes having high crystallinity for high conducting and mechanical properties under various humidified conditions. *J. Mater. Chem. A* **2015**, *3*, 20983−20991.
(39) Hergenrother, P. M.; Jensen, B. J.; Havens, S. J. Poly(arylene ethers). *Polymer* **1988**, *29*, 358−369.
(40) Walker, K. A.; Markoski, L. J.; Moore, J. S. Processible poly(arylene ether ketones) that can be crosslinked to high-performance networks. *Macromolecules* **1993**, *26*, 3713−3716.
(41) Cao, J.; Su, W.; Wu, Z.; Kitayama, T.; Hatada, K. Synthesis and properties of poly(ether ether ketone)-poly(ether sulfone) block copolymers. *Polymer* **1994**, *35*, 3549−3556.
(42) Lin, C. H.; Li, C. M.; Hsu, C. K.; Chang, H. C.; Juang, T. Y. Facile synthesis of high-performance poly(pyrrolone imide)s from an unsymmetric phosphinated triamine. *J. Polym. Sci., Part A: Polym. Chem.* **2013**, *51*, 2709−2715.
(43) Lin, C. H.; Chang, S. L.; Wei, T. P. High-T_g transparent poly(ether sulfone)s based on phosphinated bisphenols. *Macromol. Chem. Phys.* **2011**, *212*, 455−464.
(44) Lee, C. H.; Park, H. B.; Lee, Y. M.; Lee, R. D. Importance of proton conductivity measurement in polymer electrolyte membrane for fuel cell application. *Ind. Eng. Chem. Res.* **2005**, *44*, 7617−7626.
(45) Lo, C.-Y.; Li, S.; Tan, D.; Pan, M.-H.; Sang, S.; Ho, C.-T. Trapping reactions of reactive carbonyl species with tea polyphenols

https://doi.org/10.1021/acsomega.1c04205
ACS Omega 2021, 6, 35315−35324

on simulated physiological conditions. *Mol. Nutr. Food Res.* **2006**, *50*, 1118−1128.
(46) Petreus, O.; Lisa, G.; Avram, E.; Rosu, D. Thermal degradation and pyrolysis study of phosphorus-containing polysulfones. *J. Appl. Polym. Sci.* **2011**, *120*, 3233−3241.
(47) Xie, X.; Wang, Z.; Zhang, K.; Xu, J. Novel phosphorous−nitrogen containing poly(aryl ether ketone)s: Synthesis, characterization, and thermal properties. *Des. Monomers Polym.* **2013**, *16*, 38−46.
(48) Chen, H.; Zhang, K.; Xu, J. Synthesis and characterizations of novel phosphorous−nitrogen containing poly(ether sulfone)s. *Polym. Degrad. Stab.* **2011**, *96*, 197−203.
(49) Kim, D. S.; Robertson, G. P.; Kim, Y. S.; Guiver, M. D. Copoly(arylene ether)s containing pendant sulfonic acid groups as proton exchange membranes. *Macromolecules* **2009**, *42*, 957−963.
(50) De Almeida, S. H.; Kawano, Y. Thermal behavior of Nafion membranes. *J. Therm. Anal. Calorim.* **1999**, *58*, 569−577.
(51) Surowiec, J.; Bogoczek, R. Studies on the thermal stability of the perfluorinated cation-exchange membrane Nafion-417. *J. Therm. Anal.* **1988**, *33*, 1097−1102.
(52) Kim, Y. S.; Dong, L.; Hickner, M. A.; Pivovar, B. S.; McGrath, J. E. Processing induced morphological development in hydrated sulfonated poly(arylene ether sulfone) copolymer membranes. *Polymer* **2003**, *44*, 5729−5736.
(53) Roy, A.; Hickner, M. A.; Yu, X.; Li, Y.; Glass, T. E.; McGrath, J. E. Influence of chemical composition and sequence length on the transport properties of proton exchange membranes. *J. Polym. Sci., Part B: Polym. Phys.* **2006**, *44*, 2226−2239.
(54) Dai, W.; Wang, H.; Yuan, X.-Z.; Martin, J. J.; Yang, D.; Qiao, J.; Ma, J. A review on water on water balance in the membrane electrode assembly of proton exchange membrane fuel cells. *Int. J. Hydrogen Energy* **2009**, *34*, 9461−9478.
(55) Bauer, F.; Denneler, S.; Willert-Porada, M. Influence of temperature and humidity on the mechanical properties of Nafion® 117 polymer electrolyte membrane. *J. Polym. Sci., Part B: Polym. Phys.* **2005**, *43*, 786−795.
(56) Jang, H.-R.; Yoo, E.-S.; Kannan, R.; Kim, J.-S.; Lee, K.; Yoo, D. J. Facile tailor-made enhancement in proton conductivity of sulfonated poly(ether ether ketone) by graphene oxide nanosheet for polymer electrolyte membrane fuel cell applications. *Colloid Polym. Sci.* **2017**, *295*, 1059−1069.
(57) Lee, K. H.; Chu, J. Y.; Kim, A. R.; Nahm, K. S.; Kim, C.-J.; Yoo, D. J. Densely sulfonated block copolymer composite membranes containing phosphotungstic acid for fuel cell membranes. *J. Membr. Sci.* **2013**, *434*, 35−43.
(58) Kim, B.; Kannan, R.; Nahm, K. S.; Yoo, D. J. Development and characterization of highly conducting nonfluorinated di and triblock copolymers for polymer electrolyte membranes. *J. Dispersion Sci. Technol.* **2016**, *37*, 1315−1323.
(59) Balog, S.; Gasser, U.; Mortensen, K.; Gubler, L.; Scherer, G. G.; Ben youcef, H. Correlation between morphology, water uptake, and proton conductivity in radiation-grafted proton-exchange membranes. *Macromol. Chem. Phys.* **2010**, *211*, 635−643.

https://doi.org/10.1021/acsomega.1c04205
ACS Omega 2021, 6, 35315−35324